Not to appear in Nonlearned J., 45.
Preprint typeset using LaTeX style emulateapj v. 01/23/15

THE RELATIONSHIP BETWEEN SIZE AND STAR FORMATION IN ACTIVE GALAXIES

J. I. Phillips[1,2,3] and Claudia Scarlata [1]
Minnesota Institute for Astrophysics, University of Minnesota, Minneapolis, MN 55455
Not to appear in Nonlearned J., 45.

ABSTRACT

We examine a sample of SDSS galaxies with masses between $10^{8.5}$ and $10^{10.5}$ for signatures of radial feedback driven by bursty star formation. We measure each galaxy's offset from the median size-mass relation, and plot this excess size against their $H\alpha$ emission. Below $10^{9.5}$, we see a negative correlation between galaxy size and $H\alpha$ emission, i.e., actively star-forming galaxies are more compact. This is strong observational evidence for a "breathing" mode of star formation, where intense star formation in the galactic center drives radial outflows of gas and stars in a cyclic fashion. More massive galaxies do not show the same correlations between size and star formation activity, consistent with the observations that these objects reside in cuspy dark matter halos. Additionally, we examine the radial profile of star formation in both dwarf and massive galaxies, finding star formation far more concentrated in dwarf galaxies.

1. INTRODUCTION

Dwarf galaxies, galaxies at or below stellar mass of $\sim 10^{9.5} M_{\odot}$, are important laboratories that allow us to study structure formation at the smallest scales. In particular, their ratios of baryons to dark matter are extremely low, typically around 1:100. This gives rise to important differences in the structure and star formation histories of dwarf galaxies as compared to more massive galaxies, and studying these differences can shed light on important physics related to how galaxy formation is regulated by both baryons and dark matter.

Cosmological simulations based on the preferred cold dark matter model (ΛCDM) predict that galaxies form in self-similar halos of dark matter, which have density profiles described by a double power law with an inner logarithmic slope of -1, termed a Navarro-Frank-White (NFW) profile (Navarro et al. 1997). The distribution statistics and kinematics of massive galaxies is fully consistent with them living in dark matter halos with NFW profiles (Wambsganss et al. 2004; Springel et al. 2005; Boylan-Kolchin et al. 2009; Klypin et al. 2011); however, dwarf galaxy kinematics are better described by halos with a flat inner slope, typically referred to as a "cored" profile (Moore 1994; McGaugh et al. 2001; Marchesini et al. 2002; Simon et al. 2005; de Blok et al. 2008). This tension between predictions made from ΛCDM and observations is termed the "core-cusp problem." A closely related problem, the "too big to fail problem," notes that satellite halos (or subhalos) seen around Milky-Way-like galaxies in ΛCDM simulations are too dense to host any of the observed Milky Way dwarf satellites (Boylan-Kolchin et al. 2011, 2012). Note that these two problems may indeed be two manifestations of the same problem, i.e., both problems may be solved if halos in the real Universe have cored profiles. Recent work by Garrison-Kimmel et al. (2014) demonstrated that the "too big to fail" problem extended beyond the Milky Way's virial radius, suggesting that the problem has more to do with how dwarf galaxies form than how environmental effects such as ram-pressure stripping or tidal interactions manifest (See, e.g., Gunn & Gott (1972); Larson et al. (1980); Farouki & Shapiro (1981); Moore et al. (1996); Balogh et al. (2000) for a discussion of these effects).

In order to resolve these problems, one of two things must be true. Either the underlying physics of ΛCDM must be modified in some way, or baryonic processes must be invoked to bridge the gap between theory and observation. Recent work has been dedicated to exploring both possibilities. On the cosmological side, both self-interacting dark matter and warm dark matter can serve to suppress structure formation and lower the central densities of dark matter halos (Lovell et al. 2014; Elbert et al. 2015). With respect to baryonic matter, supernova feedback has long been known to deposit energy into the interstellar medium (ISM), driving galactic winds (Larson 1974; Dekel & Silk 1986). More recently, this feedback has been posited as a mechanism by which energy may be injected into dark matter particles, kinematically warming them. Several authors have argued that if star formation proceeds in bursts in dwarf galaxies, energy will be injected with enough efficiency to create cores in the centers of dark matter halos (Governato et al. 2010, 2012; Pontzen & Governato 2012a). Observational studies have demonstrated that, for dwarf galaxies in particular, the star formation rate as measured by $H\alpha$ has more scatter than the star formation rate as measured by FUV emission (Sullivan et al. 2000; Boselli et al. 2009; Lee et al. 2009; Shivaei et al. 2015; Guo et al. 2016; Sparre et al. 2017). Since these indicators trace star formation over different timescales, these studies are consistent with a picture where star formation in dwarfs is stochastically bursty; however, radial transport driven by this stochastic star formation remains unobserved.

One clue to resolving this dilemma may lie in how dwarf galaxies' old stars are distributed. While exceptions abound, massive galaxies generally have concentrations of old stars in the center, and younger stars in the outskirts (de Jong 1996; Bakos et al. 2008). Dwarf galaxies, on the other hand, typically show the inverse; young stars in the center and old stars on the outskirts (Hidalgo et al. 2009, 2013). Several studies have argued that these radial age gradients arise from in situ formation; old stars in the external region were born there at early times and generally remained there, exhibiting only minor radial movement with no preferred direction (Stinson et al. 2009; Schroyen et al. 2013). However, recent simulations have raised the possibility that stars in dwarf galaxies experience significant radial transport; young stars are born in galactic interiors, then at some point in their lifetimes they move to larger radii, possibly driven by feedback (González-Samaniego et al. 2016; El-Badry et al. 2016). Distinguishing between these two possibilities could shed light on the physics behind dwarf galaxy formation.

A unified model of galaxy formation that solves these problems was first put forward by Navarro et al. (1996), where the authors show that feedback driven outflows can produce galaxies in simulations with realistically cored profiles. Further studies (Governato et al. 2010, 2012; Maxwell et al. 2012; Di Cintio et al. 2014; Pontzen & Governato 2014; Chan et al. 2015; El-Badry et al. 2016) refined the theory, specifying that feedback regulates dwarf galaxy star formation in a stochastic manner and powers radial transport, but an observational smoking gun for this model remains elusive.

In this study, we use observations of both dwarf galaxies and massive galaxies to investigate the observational predictions of a model for dwarf galaxy formation whereby stochastic star formation in the center of the galaxy powers radial transport of both baryonic and dark matter. Specifically, our study will focus on the structure of star forming galaxies, and how that structure is dependent on the vigor with which the galaxy is forming stars. [Description of sections]. Throughout the paper we use h=0.7 in appropriate calculations, and unless otherwise noted, star formation rates are calculated according to Kennicutt (1998).

2. DATA AND OBSERVATIONS

The data used in this study come from the Sloan Digital Sky Survey (SDSS, York et al. 2000), making use of the NYU and MPA-JHU value-added galactic catalogs (Kauffmann et al. 2003; Brinchmann et al. 2004; Blanton et al. 2005). To select our scientific sample, we first take all galaxies with stellar masses between $10^{8.0}$ and $10^{11.0} M_{\odot}$. We require galaxies in our scientific sample to be actively star forming, so we impose a minimum $H\alpha$ equivalent width of 2Å and require that the galaxies we select reside in the purely star forming region of the BPT diagram (Baldwin et al. 1981). We admit to the scientific sample only galaxies within a mass-dependent completeness redshift, estimated by dividing the sample into six mass bins of width 0.5 dex and plotting a histogram of the redshift of galaxies in each bin. The peak of the histogram was taken to be the approximate completeness limit for the scientific sample. These limits, as well as the number of galaxies in our sample, are given in Table 2.2.

2.1. *Central star formation*

SDSS spectroscopy is based on light being channeled into fibers 3 arcsec in diameter. This gives us an opportunity to more closely probe the star formation rate in the galaxy's central regions. Since we will be interested in star formation happening in the galaxy's center, we will define a fiber-corrected star formation rate that intentionally overly relies on measurements at the galaxy center, which we will call $\mathrm{SFR_{cent}}$. Eventually, we will be interested in whether or not $\mathrm{SFR_{cent}}$ is larger or smaller than the galaxy's true star formation rate, which will give us a measure of how centrally concentrated the star formation is, but first we will detail how $\mathrm{SFR_{cent}}$ is calculated.

We begin by defining a parameter Ψ that corresponds to the fraction of a galaxy's area on the sky that lies within the fiber. For galaxies smaller than 3 arcsec, $\Psi = 1$. For larger galaxies, $\Psi = \frac{\pi R^2}{A_z}$, where R is the circularized radius of the galaxy measured in kpc (taken to be r-band R90 so as to account for nearly all light from the galaxy) and A_z is the area of a circle of diameter 3 arcsec at the redshift of the galaxy. Figure 1 shows Ψ plotted against galaxy radius for galaxies in our $10^{9.5} - 10^{10.0}$ bin. Notice that, as one might expect, larger galaxies tend to have more of their area fall outside out the fiber, leading to lower values of Ψ. The selection effect in the upper right portion of the plot is introduced by the redshift cut we place on the sample. An object that lies on this line is located close to the maximum allowed redshift, such that it is the minimum size on the sky, and thus the largest Ψ.

If we are carrying out a correction on some generic parameter Θ, which could represent e.g. star formation rate, we assume that the correction will take the form of a power law, i.e.,

$$\Theta_{\mathrm{total}} = \Theta_{\mathrm{fiber}} \times \Psi^{-\alpha}$$

. Here α is a power law index that we will derive empirically and Θ_{fiber} is the measured value of Θ within the fiber. In calculating α, our goal is to correct Θ such that its distribution is independent of redshift. We assume no redshift evolution within our full sample, which is a fair assumption between z=0 and z=0.07. To this end, we fit a linear relationship to $log\Theta_{fiber}$ and $log\Psi$. The slope of this relationship we adopt as α.

To validate that our correction procedure does indeed produce a measure for Θ that is independent of redshift, we divide each mass bin on redshift. We will refer to these as the low redshift subsample and high redshift subsample[1]. Galaxies with redshift less than $z_{complete}/2$ are placed in the low redshift subsample, and with redshifts between $z_{complete}/2$ and $z_{complete}$ in the high redshift sample. In applying the correction, we will call the measured value of the parameter of interest Θ_{fiber}. We then compare at the distributions in Θ_{total} between the low and high redshift sample. This comparison is shown in H_{α} luminosity in Figure 3 for the $M\star\ 10^{9.5} M_{\odot}$ bin. We see excellent agreement in the corrected values across redshift for each mass bin, and note that this agreement is only seen after the correction is made. Table **??** contains the measured alphas and completeness redshifts for each sample. If we substitute SFR for the generic Θ in the above derivation, we can make explicit the definition

$$SFR_{cent} \equiv SFR_{fiber} \times \Psi^{-alpha}$$

.

2.2. *Concentration/luminosity degeneracy*

[1] We use "high" redshift in a relative sense; all galaxies we consider in this paper are quite low redshift.

Mass Bin ($M_\odot$)	α	$z_{\rm complete}$	N
$10^{8.0} - 10^{8.5}$	1.347	0.023	4376
$10^{8.5} - 10^{9.0}$	0.797	0.023	13732
$10^{9.0} - 10^{9.5}$	0.830	0.035	29979
$10^{9.5} - 10^{10.0}$	0.895	0.058	58709
$10^{10.0} - 10^{10.5}$	0.698	0.081	88476
$10^{10.5} - 10^{11.0}$	0.731	0.15	69858

Table 1
Power law index and completeness redshift for galaxies in each mass bin we consider.

As previously mentioned, the above procedure produces a measure for SFR_{cent} that is overly reliant on information from the galaxy's center. If two galaxies have the same Ψ and SFR_{fiber}, they would end up with the same SFR_{cent}, even if one of them had substantially more star formation in its outskirts (and thus a higher true star formation rate). Essentially, using the parameter SFR_{cent} introduces a degeneracy between a galaxy's true star formation rate and the concentration of its star formation. Note that, had we simply corrected for the area outside of the fiber (i.e., applied an $\alpha = 1$ correction), we would have been degenerate in redshift as well.

To investigate this degeneracy, we carried out a simple Monte Carlo simulation with toy models of galaxies. The galaxies were divided into an inner and outer region, each with a separate star formation density. Galaxies were divided into two categories: those with greater star formation rate density in the center, and those with greater star formation rate density in the outskirts; i.e. galaxies with central star formation and galaxies with star formation in the disk. We then applied the same steps described above to determine a SFR_{cent} for our simulated galaxies. Upon plotting SFR_{cent} vs. Ψ, the two models occupy distinct regions of parameter space, with the objects centrally concentrated star formation displaying the highest SRF_{cent} and the objects with low central star formation displaying the lowest. To remove the variation due to intrinsic star formation, we normalize SFR_{cent} by each galaxy's intrinsic star formation rate. This allows us to examine $\log\frac{\rm SRF_cent}{\rm SFR}$ for each galaxy as the "central excess" in star formation. If we color the points in $\log\frac{\rm SRF_cent}{\rm SFR}$ vs. Ψ space by concentration (i.e., R90/R50) we can see a correspondence between high $\log\frac{\rm SRF_cent}{\rm SFR}$ and concentration. We will therefore use this ratio as a proxy for the concentration of star formation in our galaxies. Note that while $\log\frac{\rm SRF_cent}{\rm SFR}$ can serve as a proxy for concentration, we can not establish a one-to-one mapping between $\log\frac{\rm SRF_cent}{\rm SFR}$ and concentration.

3. RESULTS

In this section we will examine the relationship between a galaxy's physical size (as probed by r-band R90) and the rate and concentration of its star formation. Our sample is divided into bins of 0.5 dex in stellar mass, allowing us to examine how the relationship between size and $H\alpha$ emission with galaxy mass. Of particular interest is what happens at dwarf-scale masses, i.e., the lower-mass half of our sample.

To establish a mass-independent size metric, we fit a mass-size relation to all star-forming galaxies below redshift 0.03, then determine the expected size for each galaxy in the sample based on its stellar mass. For each galaxy, we then calculate a "size offset" which is the logarithm of the ratio between the actual size of the galaxy in kpc and the expected size of that galaxy, also in kpc. This size offset parameter has the useful properties of being centered at or very close to zero for any given population of galaxies, and having relatively consistent scatter (about 0.4 dex) over the mass ranges we probe.

In Figure 5, we plot star formation rate against size offset for galaxies in each mass bin. As expected, star formation tends to increase with increasing mass. Within each mass bin, we plot the average star formation rate at fixed size offset as a blue line. The broad trend we see is a decreasing slope from the lowest mass bin to the highest, such that smaller galaxies are less star forming at lower masses.

If, however, we plot the slope of our size/star formation rate relation against the stellar mass of the galaxies in each bin (Figure 6), we see a more complicated behavior. Rather than monotonically decreasing with stellar mass, the slope turns over $10^{8.5}M_\odot$ and again at $10^{9.5}M_\odot$. The size of the error bars makes it unclear whether or not the turnover at $10^{8.5}M_\odot$ is indeed real, however the turnover at $10^{9.5}M_\odot$ seems to indeed be real.

We see a very similar result when we examine the star formation rate density with respect to size and mass. Figures 7 shows the average star formation rate density plotted against size offset for galaxies in our six bins, while Figure 8 shows the dependence of the slope of that relation on galactic stellar mass. Unsurprisingly, we see essentially the same trends, with a strong maximum at $10^{9.5}M_\odot$ and a weak minimum at $10^{8.5}M_\odot$.

It should be said that this effect is somewhat subtle. Even the largest discrepancy in star formation between small and large galaxies we observe results in only a 20% boost in star formation for larger galaxies. On the other hand, the equivalence of star formation rate between large and small galaxies in the lowest mass bin corresponds to a $\sim$ 15% larger average star formation rate density in the smaller objects. While these changes in star formation rate are not large, they are statistically significant due to the high number of galaxies in our sample.

3.1. *Central Star Formation*

In section 2.2, we discuss how the ratio $\log\frac{\rm SRF_cent}{\rm SFR}$, which describes the deviation in total star formation implied by the galaxy's center from the true star formation rate, can be used to probe galaxy concentration. We turn now to examining how this ratio varies with galaxy size and mass.

In Figure 9, we plot the relationship between $\log\frac{\rm SRF_cent}{\rm SFR}$ and size offset for galaxies in the six mass bins, showing the relation between the slopes of these relations and stellar mass in Figure 10. We see again two inflection points, this time at $10^{8.5}M_\odot$ and $10^{10.0}M_\odot$. Again, the lower inflection point relies heavily on the uncertain value of the point at $10^{8.5}M_\odot$; however, the inflection point at higher masses seems robust. Overall, the trend is that objects at intermediate mass, i.e. between $10^{9.0}M_\odot$ and $10^{10.0}M_\odot$ exhibit higher concentrations in smaller objects than is seen in other mass bins.

In Figure 11, we plot $\frac{SRF_{cent}}{SFR}$ versus size offset for the $10^{9.5}M_\odot$ mass bin. Under the assumption that the total

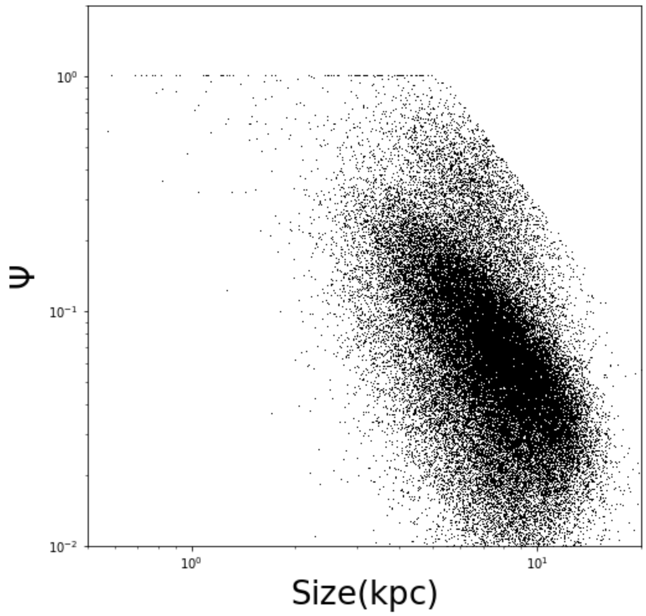

Figure 1. Geometric parameter Ψ plotted vs. physical size for galaxies in the $10^{10} - 10^{10.5} M_\odot$ mass bin. Ψ measures the fraction of the galaxy that falls within the SDSS fiber. The selection effect arises due to the cut in redshift space.

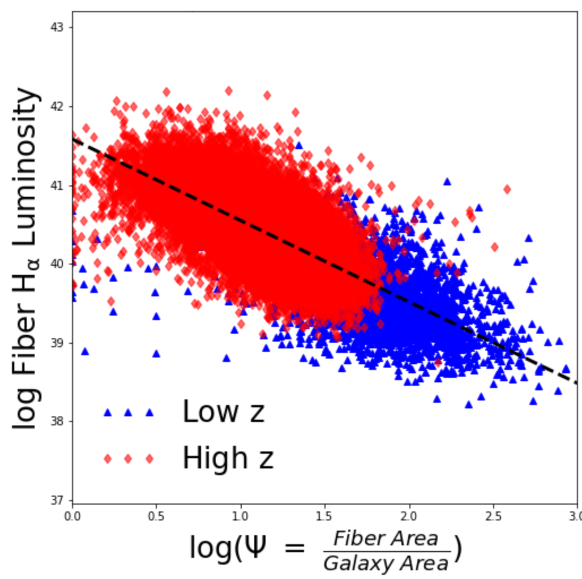

Figure 2. The relationship between the geometric factor Ψ measuring the ratio of a galaxy's size to the size of the SDSS fiber and the fiber H_α luminosity for galaxies in the $10^{9.5} - 10^{10} M_\odot$ bin. Knowing the average functional form of this relationship allows us to correct for fiber effects. Points marked with a blue triangle are at lower redshift than those marked with a red diamond

distribution is a sum of two distributions representing the active and passive components, we model the total distribution as a mixture of two Gaussian processes using the python package SKLEARN. These results are shown in the figure; the line through the two dimensional histogram separates the two Gaussian distributions, which we interpret as objects in the active and passive phases respectively. We can estimate of the fraction of time each object spends in the active phase to be equal to the fraction of objects observed to be in the active phase, which we measure as 0.43. This measurement is reasonably robust to the precise method of dividing the sample into its active and passive components. In Section 4, we will use this value to comment on the physics at play in these systems.

4. DISCUSSION

4.1. *Galaxy Size*

An important prediction of the "breathing" model of feedback regulation in dwarf galaxies is that star formation rate is anticorrelated with galaxy size. In the model, stars are formed in the galactic center. The young stars

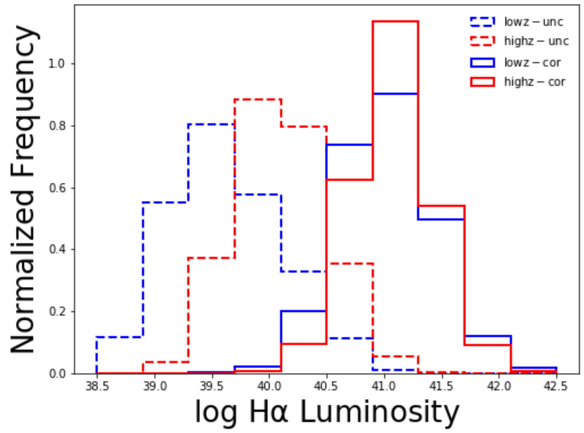

Figure 3. Histogram of $H\alpha$ luminosities for the uncorrected (dashed blue line) and corrected (solid blue line) low z calibration set, along with the uncorrected (dashed red line) and corrected (solid red line) high z calibration set. Correcting both sets brings them into agreement.

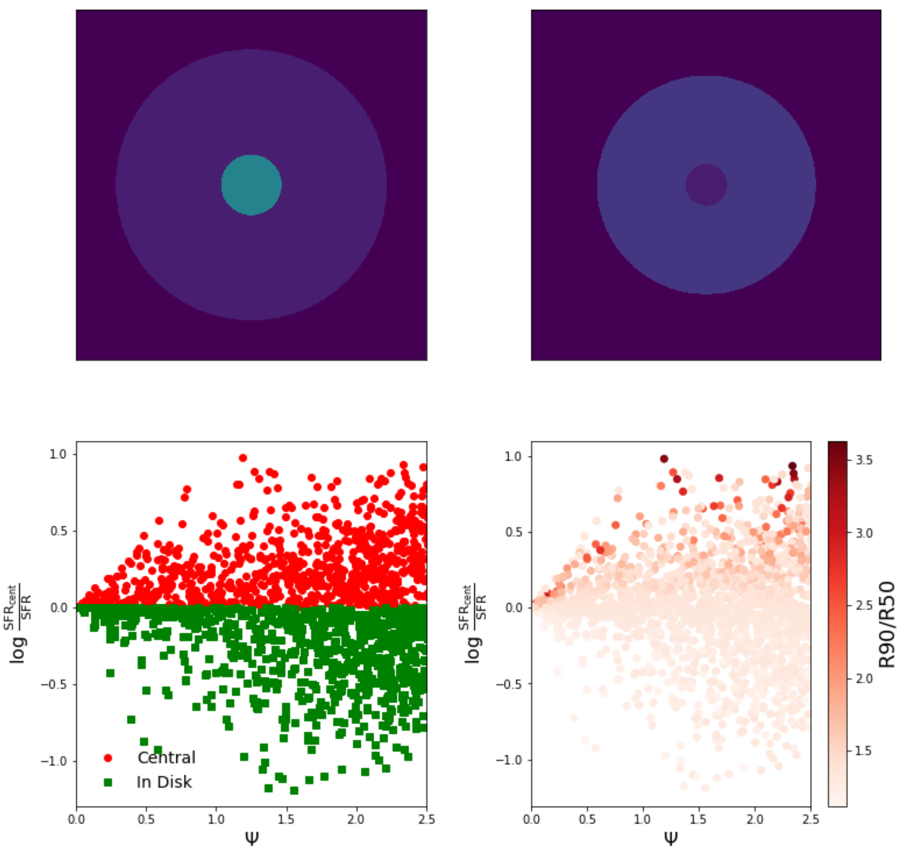

Figure 4. *Top:* Examples of allowed toy star-forming models; *left*: centrally concentrated star formation, *center*: constant star formation density, *right*: star formation preferentially in the outskirts. *Bottom:* log $\mathrm{SFR_{cent}}$ vs. Ψ colored by (*left*) model, and (*right*) concentration.

then produce supernova feedback, which blows out the reservoir of gas from which the stars were formed, dampening star formation. As a result, galaxies are actively forming stars when they are at their smallest. During the subsequent blowout phase the galaxy will be more diffuse and, if the galactic wind drives radial transport, the galaxy will have a larger effective radius (El-Badry et al. 2016).

Our results give compelling evidence for this prediction below $10^{9.5}M_{\odot}$, suggesting that dwarf galaxies form stars in a "breathing" mode. Furthermore, we see enhanced concentration in the interiors of smaller dwarf galaxies in the high-mass dwarf mass range, suggesting they are in compact active phases. Taken together, these provide evidence for a breathing mode of feedback-regulated star formation in high-mass dwarfs.

We can also examine the mass ranges at which we see effects with galaxy size to the mass ranges related to the interplay between feedback and potential well depth. In Figure 12, we plot the slope of the $\frac{SFR_{cent}}{SFR}$ relation

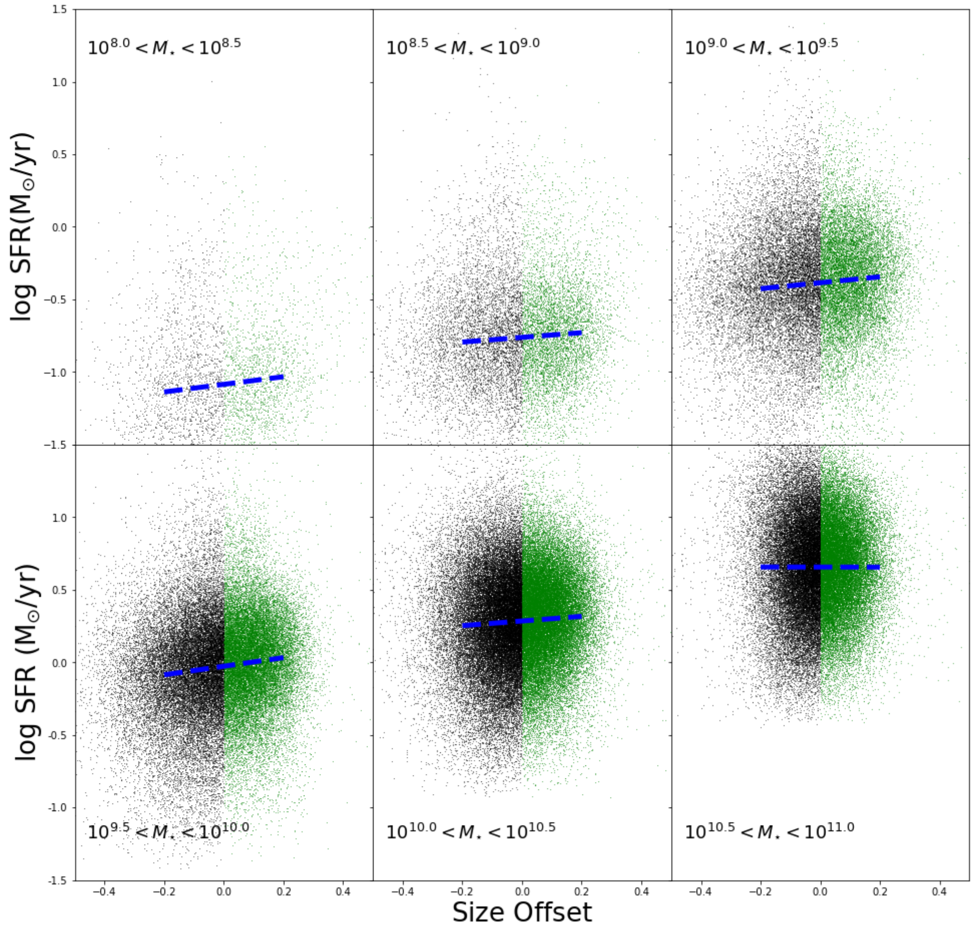

Figure 5. Star formation rate plotted against size offset for galaxies in six mass bins. The data transition from a nearly flat relation at small masses to a slight correlation at larger masses. Black and green points represent smaller-than-average and larger-than-average galaxies, respectively. Blue dashed line is a linear fit to the data.

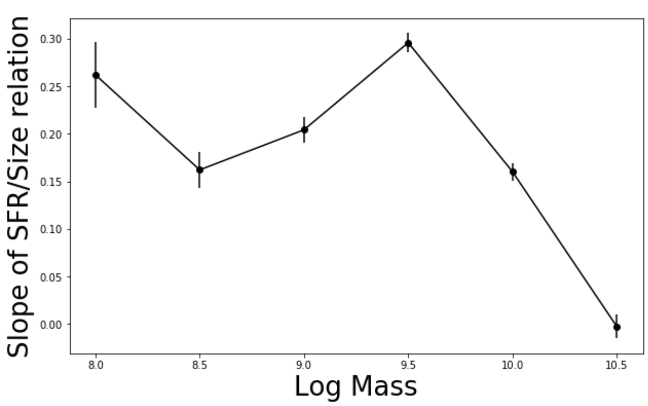

Figure 6. Slope of the star formation rate vs. size relation plotted against stellar mass.

against stellar mass alongside the mass outflow rate normalized by halo mass. We see that both plots have inflection points around $10^9 M_\odot - 10^9 M_\odot$, suggesting that this mass range is important for both plots. Indeed, the knee of the outflow rate relation lines up well with the mass range at which small galaxies no longer have an excess in concentration in their star formation, potentially indicating a mass scale at which the breathing model no longer operates.

There are, however, potential alternate explanations for the observed effects we point out. We will briefly discuss these. Firstly, we will consider the possibility that galaxies at different sizes do form stars at the same rate, but different amounts of $H\alpha$ emission escape the galaxy. This could be due to variations in the initial mass function (IMF), which sets the rates at which stars of different masses form. A top-heavy IMF, where more massive stars are formed relatively more frequently, would result in more ionizing radiation being formed per unit star formation. Our results could potentially be explained by smaller galaxies having more top-heavy IMFs. Whether or not the IMF varies between galaxies, or within galaxies, is an area of active research, with most results being consistent with a universal IMF (e.g., Lee et al. 2009; Bastian et al. 2010).

An alternate possibility is that galaxies form stars at the same rate and as described by the same IMF at the same mass, but dust obscures star formation in such a way as to create a trend where there would otherwise be none. However, previous studies have shown that dust reddening increases with increasing stellar mass (Garn & Best 2010), leaving it unlikely to drive an effect seen primarily at dwarf masses. We see a similar result in our data, with Balmer decrement increasing with increasing galaxy mass. Thus we conclude that dust extinction is unlikely to be the driver of the effects we see.

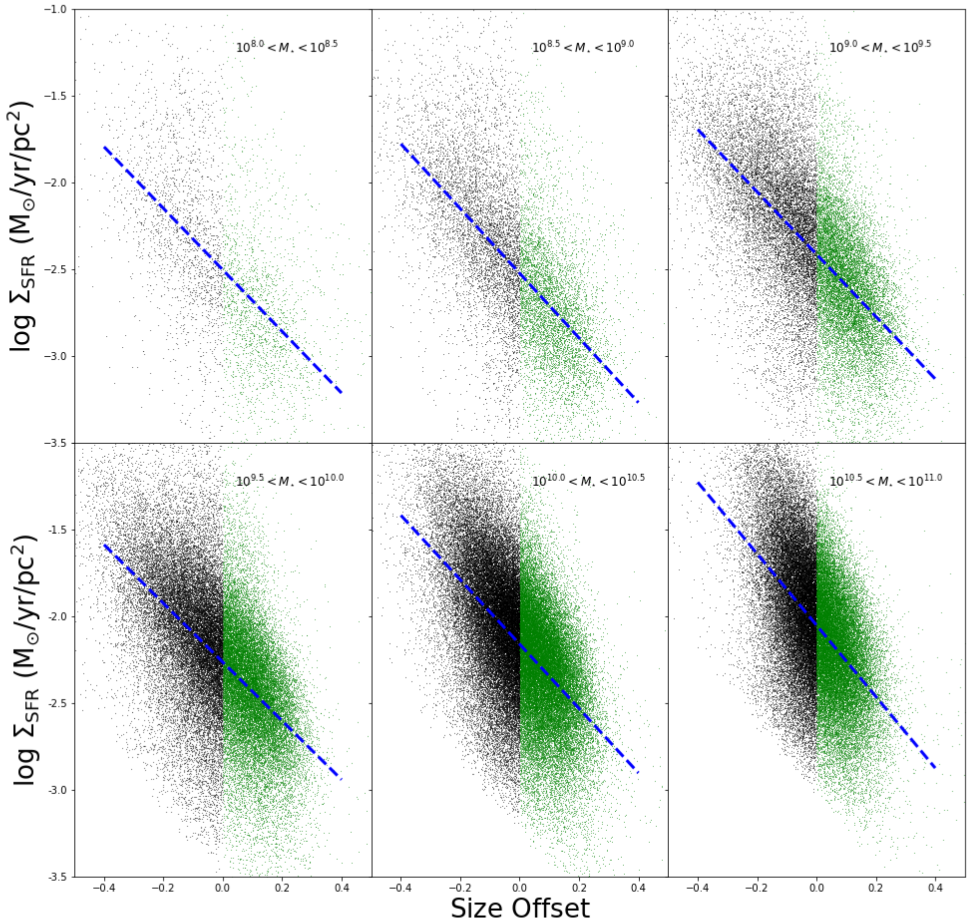

Figure 7. Star formation rate plotted against size offset for galaxies in six mass bins. The data transition from a nearly flat relation at small masses to a slight correlation at larger masses. Black and green points represent smaller-than-average and larger-than-average galaxies, respectively. Blue dashed line is a linear fit to the data.

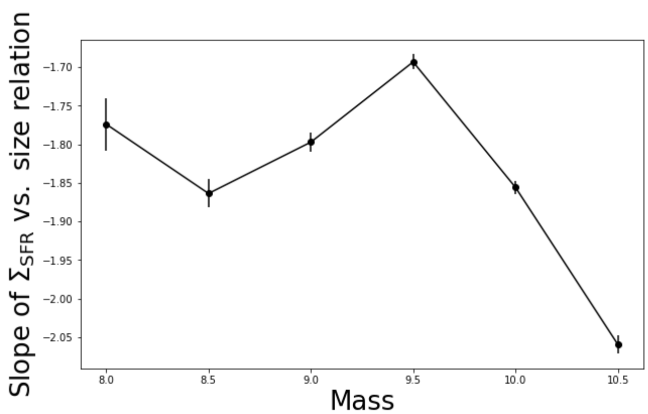

Figure 8. Slope of the star formation rate density vs. size relation plotted against stellar mass.

4.2. *Duty Cycle and Energetics*

In Section 3, we divide the galaxies in our lowest mass bin into actively and passively star forming subcategories via a Gaussian process decomposition. We draw an important distinction between *passively star forming* galaxies, which still show signs of ongoing star formation, and *passive galaxies*, which no longer are forming stars. The latter are outside the scope of this paper, having been eliminated from our sample by our H_α equivalent width cut. We define the duty cycle of this population to be the fraction of time a galaxy spends in its active phase, as estimated by the fraction of galaxies observed to be in the active phase, and measure this value to be 0.42; i.e., dwarf galaxies spend roughly forty percent of their lifespan in a phase where they are actively forming stars and the other sixty percent not in this phase. Due to the increased size of the galaxy during the passively star forming phase, we will interpret this to be the phase where the galaxy is undergoing stellar feedback-driven blowouts. There are several different interpretations for this measured duty cycle that we now discuss.

Firstly, we will examine this number under the view that the instantaneous star formation rate in dwarf galaxies at a particular time is a stochastic sampling of an underlying probability distribution of star formation rates. Of course, this view is only sensible as an approximation; nevertheless, there are benefits to thinking of star formation in this way, particularly as it pertains to generating analytic and semi-analytic models (Kelson et al. 2016).

Under this probabilistic interpretation, a galaxy's star formation rate represents a sampling of an underlying star formation rate probability distribution function. Our result suggest that the probability of galaxies being in the quiescent state is twice as high as the galaxies in the active state. We draw a distinction between

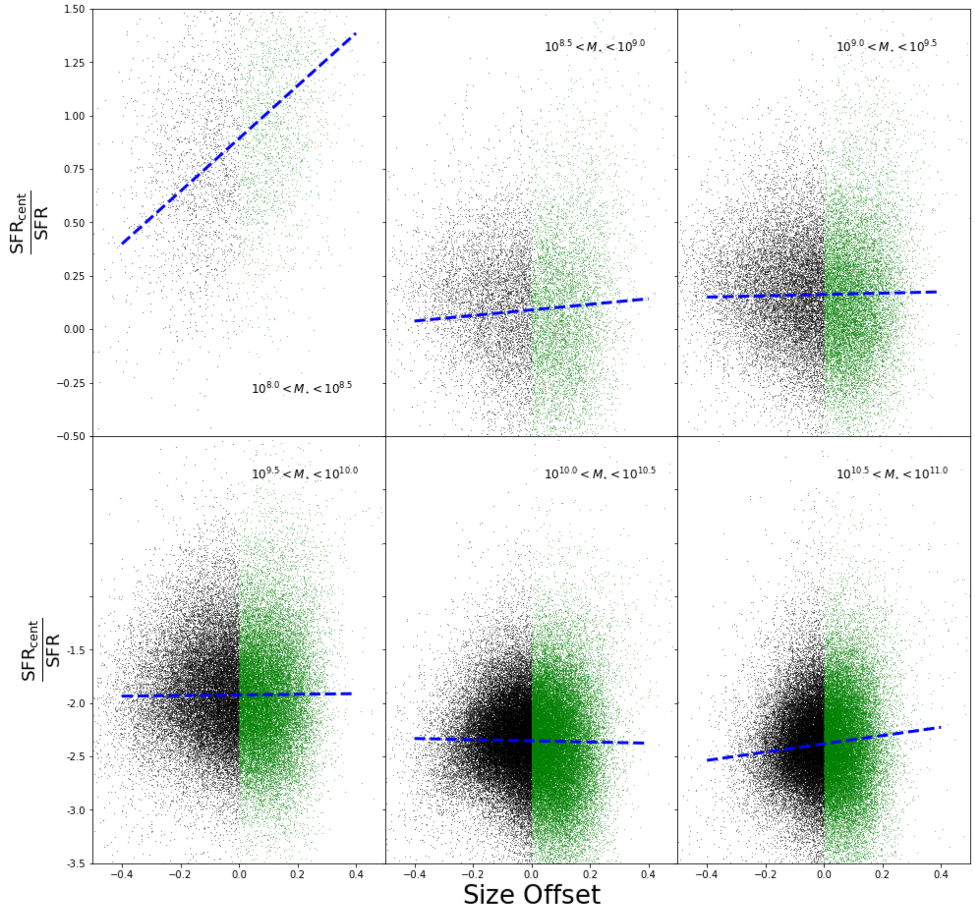

Figure 9. Star formation rate plotted against size offset for galaxies in six mass bins. The data transition from a nearly flat relation at small masses to a slight correlation at larger masses. Black and green points represent smaller-than-average and larger-than-average galaxies, respectively. Blue dashed line is a linear fit to the data.

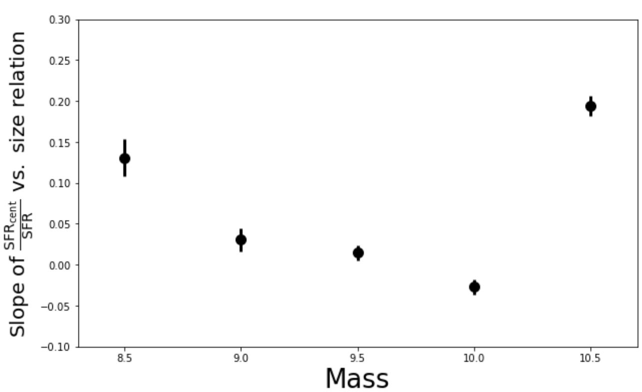

Figure 10. Slope of the star formation rate vs. size relation plotted against stellar mass.

this quiescent phase and final quenching, when a galaxy becomes "red and dead." This final quenching phase is likely not a result of stochastic sampling of an underlying pdf, but rather the result of physical processes that bring the galaxy out of the "breathing" mode and into the "red and dead" mode. In particular, galaxies at these masses are predominantly quenched through environmental means (Kauffmann et al. 2003; Geha et al. 2012).

Physically, we can interpret duty cycle in terms of the times a galaxy spends in each phase in order to explore the physicals scalings and energetics involved. As an example, we use the test case of a $10^9 M_\odot$ galaxy of radius 5 kpc. Assuming that the blowout moves with the speed v_{wind}, the total time it takes to reach the edge of the galaxy is $\frac{R}{v_{wind}}$. If the material takes the same amount of time to fall back onto the center as to reach the galactic outskirts, then the total time spent in the passive phase is twice this time. Using the duty cycle implied by Figure 11, we can conclude empirically that the time spent in the active phase during a single burst is

$$t_{active} = \frac{4 \times R}{5 \times v_{wind}} = 13.0 Myr \times \frac{R}{5kpc} \times \frac{300 km/s}{v_{wind}}$$

, consistent with the timescales put forward by El-Badry et al. (2016). Multiplying this value by the star formation rate of objects in the active phase gives us the total number of stars formed in one cycle:

$$\Delta M_\star = 6.4 \times 10^5 M_\odot \times \frac{SFR}{0.062 M_\odot/yr} \times \frac{t_{active}}{13.0 Myr}$$

.

The IMF allows us to connect the amount of star formation in a burst to the strength of the supernova feedback produced by that burst. Under a Kroupa IMF (Kroupa 2002), we expect one Type II supernova for every 100 solar masses in stars formed, meaning that a single burst in a dwarf galaxy produces some 8×10^3

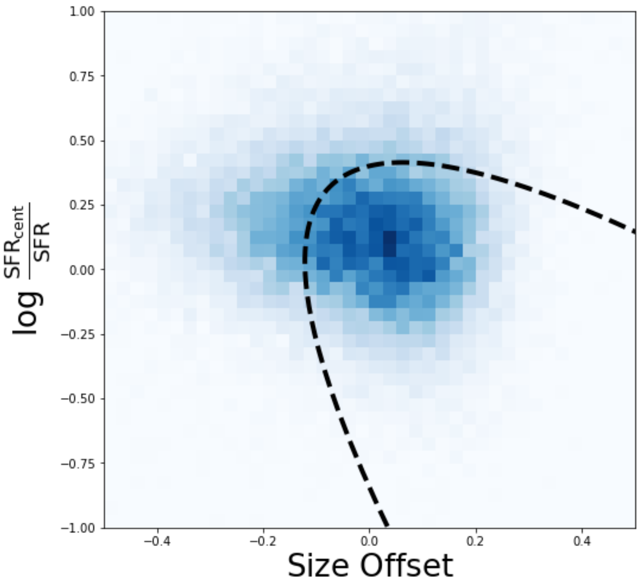

Figure 11. Black line divides the lowest mass sample into actively and passively star-forming galaxies as derived from a Gaussian mixture model. Approximately 57% of the sample is in the passive regime, while 43% is in the active regime.

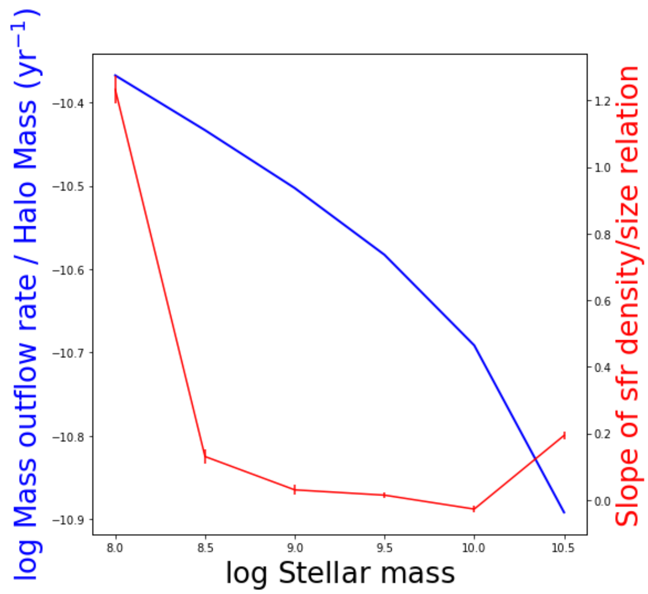

Figure 12. *Red line:* Slope of star formation rate surface density vs. size relation plotted against stellar mass. *Blue line:* Mass outflow rate per unit dark matter halo mass plotted against stellar mass.

Type II supernova. Given that the average energy output of a Type II supernova is 10^{51} erg, the total energy output during a single burst is 10^{55} erg. In order to produce $10^9 M_\odot$ of stellar mass, the galaxy must have gone through 10^3 cycles, thereby producing 10^{58} erg of supernova energy in the process. The energetic argument presented in the above paragraph is true independent of whether the stars are formed constantly or in bursts. However, as several authors have argued (Governato et al. 2012; Garrison-Kimmel et al. 2013), the "bursty" mode of star formation can produce a positive feedback cycle, where the the efficiency of subsequent bursts increases from the initial burst (see Pontzen & Governato 2012b; Governato et al. 2012).

4.3. *Comparisons to Simulations*

Hydrodynamical simulations whereby galaxy growth is regulated through burst-driven radial transport make a number of specific, testable predictions of galaxy observables. We divide our discussion of these predictions into two sections: predictions concerning galaxy dynamics, which we do not address but is addressed by Cicone et al. (2016), and predictions concerning galaxy structure, which is the primary concern of this work.

The burst-driven transport model of galaxy self-regulation requires that feedback not only couple to the gas in a galaxy, but also to the stellar component. As a result, the stars are kinematically heated, resulting in an increased line of sight velocity dispersion. El-Badry et al. (2017) makes this prediction explicit, demonstrating a correlation between σ_{LOS} and specific star formation rate for star particles in the final 40 snapshots of one simulated dwarf galaxy halo. Under the assumption that the evolution of this single halo is an ergodic process, this supplies a prediction for the population of dwarf galaxies at low redshift.

These predictions are borne out by the analysis of Cicone et al. (2016), which uses stacked SDSS spectra to examine the profiles of nebular emission lines and stellar absorption lines, constraining the dynamics of galactic gas and stars respectively. They find that, for dwarf galaxies, the width of stellar absorption lines increases with increasing specific star formation rate, consistent with the predictions of El-Badry et al. (2017). Furthermore, they find that this trend disappears above stellar masses of $10^{9.5}M_{\odot}$, consistent with the prediction that burst-driven transport only operates at dwarf mass scales.

We can also compare the trends with size that we have explored in this work to predictions from hydrodynamical simulations. In Figure 13, we over plot the final 40 snapshots from a dwarf galaxy in the FIRE simulation with galaxies from our lowest-mass bin ($10^{8.5} - 10^{9.0} M_{\odot}$) in specific star formation rate/size space. Again, we emphasize that since the simulated galaxies evolve in this space, the points traced by the galaxy in the simulation make a prediction for galaxies sampled in the real Universe. We see agreement between the predictions made by the simulation and our observed relationship between specific star formation rate and size. There is significantly more scatter in the observed relation than the simulation results, which is a natural result of comparing an ensemble of galaxies with a single simulated object, but the overall agreement between simulations and data is striking. Taken together, these two observational confirmations of simulation predictions provide strong evidence that burst-driven radial transport is occurring in dwarf galaxies.

5. CONCLUSION

Our study primarily examines the relationship between the physical size of a galaxy and it's star formation properties. We show the following,

- Dwarf galaxies with smaller size tend to have higher levels of $H\alpha$ emission. Dwarf galaxies of larger size have lower levels of $H\alpha$ emission. This trend goes away in more massive galaxies.

- $H\alpha$ surface density is consistent with a power law with respect to radius in the inner regions of galaxies at all masses, however in dwarf galaxies, the outer regions have $H\alpha$ emission consistent with zero.

- Taken together, these results paint a picture in which dwarf galaxies experience cycles of star formation, where dense star formation in the central regions drives blowouts that self-regulate galaxy growth. Furthermore, our results are in strong agreement with simulations that exhibit such blowouts. The energy of the blowouts couples to the stars, leading to dwarf galaxies in their blowout phase being larger on the sky in the r band.

REFERENCES

Bakos, J., Trujillo, I., & Pohlen, M. 2008, ApJL, 683, L103
Baldwin, J. A., Phillips, M. M., & Terlevich, R. 1981, PASP, 93, 5
Balogh, M. L., Navarro, J. F., & Morris, S. L. 2000, ApJ, 540, 113
Bastian, N., Covey, K. R., & Meyer, M. R. 2010, ARA&A, 48, 339
Blanton, M. R., Schlegel, D. J., Strauss, M. A., et al. 2005, AJ, 129, 2562
Boselli, A., Boissier, S., Cortese, L., et al. 2009, ApJ, 706, 1527
Boylan-Kolchin, M., Bullock, J. S., & Kaplinghat, M. 2011, MNRAS, 415, L40
—. 2012, MNRAS, 422, 1203
Boylan-Kolchin, M., Springel, V., White, S. D. M., Jenkins, A., & Lemson, G. 2009, MNRAS, 398, 1150
Brinchmann, J., Charlot, S., White, S. D. M., et al. 2004, MNRAS, 351, 1151
Chan, T. K., Kereš, D., Oñorbe, J., et al. 2015, MNRAS, 454, 2981
Cicone, C., Maiolino, R., & Marconi, A. 2016, A&A, 588, A41
de Blok, W. J. G., Walter, F., Brinks, E., et al. 2008, AJ, 136, 2648
de Jong, R. S. 1996, A&A, 313, 377
Dekel, A., & Silk, J. 1986, ApJ, 303, 39
Di Cintio, A., Brook, C. B., Macciò, A. V., et al. 2014, MNRAS, 437, 415
El-Badry, K., Wetzel, A., Geha, M., et al. 2016, ApJ, 820, 131
El-Badry, K., Wetzel, A. R., Geha, M., et al. 2017, ApJ, 835, 193
Elbert, O. D., Bullock, J. S., Garrison-Kimmel, S., et al. 2015, MNRAS, 453, 29
Farouki, R., & Shapiro, S. L. 1981, ApJ, 243, 32
Garn, T., & Best, P. N. 2010, MNRAS, 409, 421
Garrison-Kimmel, S., Boylan-Kolchin, M., Bullock, J. S., & Kirby, E. N. 2014, MNRAS, 444, 222
Garrison-Kimmel, S., Rocha, M., Boylan-Kolchin, M., Bullock, J. S., & Lally, J. 2013, MNRAS, 433, 3539
Geha, M., Blanton, M. R., Yan, R., & Tinker, J. L. 2012, ApJ, 757, 85
González-Samaniego, A., Avila-Reese, V., & Colín, P. 2016, ApJ, 819, 101
Governato, F., Brook, C., Mayer, L., et al. 2010, Nature, 463, 203
Governato, F., Zolotov, A., Pontzen, A., et al. 2012, MNRAS, 422, 1231
Gunn, J. E., & Gott, III, J. R. 1972, ApJ, 176, 1
Guo, Y., Rafelski, M., Faber, S. M., et al. 2016, ApJ, 833, 37
Hidalgo, S. L., Aparicio, A., Martínez-Delgado, D., & Gallart, C. 2009, ApJ, 705, 704
Hidalgo, S. L., Monelli, M., Aparicio, A., et al. 2013, ApJ, 778, 103
Kauffmann, G., Heckman, T. M., White, S. D. M., et al. 2003, MNRAS, 341, 54
Kelson, D. D., Benson, A. J., & Abramson, L. E. 2016, ArXiv e-prints, arXiv:1610.06566
Kennicutt, Jr., R. C. 1998, ARA&A, 36, 189
Klypin, A. A., Trujillo-Gomez, S., & Primack, J. 2011, ApJ, 740, 102
Kroupa, P. 2002, Science, 295, 82
Larson, R. B. 1974, MNRAS, 169, 229
Larson, R. B., Tinsley, B. M., & Caldwell, C. N. 1980, ApJ, 237, 692
Lee, J. C., Gil de Paz, A., Tremonti, C., et al. 2009, ApJ, 706, 599
Lovell, M. R., Frenk, C. S., Eke, V. R., et al. 2014, MNRAS, 439, 300
Marchesini, D., D'Onghia, E., Chincarini, G., et al. 2002, ApJ, 575, 801
Maxwell, A. J., Wadsley, J., Couchman, H. M. P., & Mashchenko, S. 2012, ApJL, 755, L35
McGaugh, S. S., Rubin, V. C., & de Blok, W. J. G. 2001, AJ, 122, 2381
Moore, B. 1994, Nature, 370, 629
Moore, B., Katz, N., Lake, G., Dressler, A., & Oemler, A. 1996, Nature, 379, 613
Navarro, J. F., Eke, V. R., & Frenk, C. S. 1996, MNRAS, 283, L72
Navarro, J. F., Frenk, C. S., & White, S. D. M. 1997, ApJ, 490, 493
Pontzen, A., & Governato, F. 2012a, MNRAS, 421, 3464
—. 2012b, MNRAS, 421, 3464
—. 2014, Nature, 506, 171

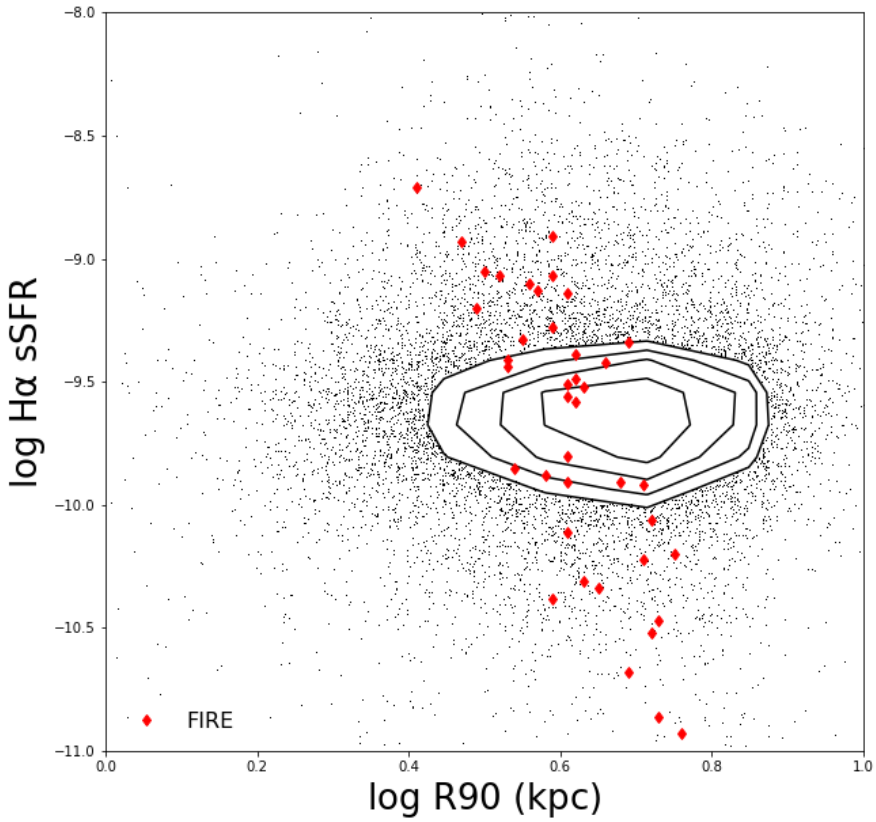

Figure 13. Star formation rate plotted against size for galaxies in our lowest mass bin. Overplotted are points from the last 40 snapshots of a dwarf galaxy in the FIRE simulation that is undergoing self-regulation via burst-driven radial transport. The data is in excellent agreement with the predictions from the simulations

Schroyen, J., De Rijcke, S., Koleva, M., Cloet-Osselaer, A., & Vandenbroucke, B. 2013, MNRAS, 434, 888

Shivaei, I., Reddy, N. A., Shapley, A. E., et al. 2015, ApJ, 815, 98

Simon, J. D., Bolatto, A. D., Leroy, A., Blitz, L., & Gates, E. L. 2005, ApJ, 621, 757

Sparre, M., Hayward, C. C., Feldmann, R., et al. 2017, MNRAS, 466, 88

Springel, V., White, S. D. M., Jenkins, A., et al. 2005, Nature, 435, 629

Stinson, G. S., Dalcanton, J. J., Quinn, T., et al. 2009, MNRAS, 395, 1455

Sullivan, M., Treyer, M. A., Ellis, R. S., et al. 2000, MNRAS, 312, 442

Wambsganss, J., Bode, P., & Ostriker, J. P. 2004, ApJL, 606, L93

York, D. G., Adelman, J., Anderson, Jr., J. E., et al. 2000, AJ, 120, 1579